Heliyon 11 (2025) e42116

Contents lists available at ScienceDirect

Heliyon

journal homepage: www.cell.com/heliyon

Case report

A novel TGFBR2 mutation causes Loeys-Dietz syndrome in a Chinese infant: A case report

Xin Liu [a,1], Kaiqing Liu [b,1], Lifu Hu [c], Zixiao Liu [a], Xinhua Liu [a,*], Jiantao Wang [a,**]

[a] Shenzhen Eye Hospital, Jinan University, Shenzhen Eye Institute, Shenzhen, China
[b] Shenzhen Luohu Hospital Group, The Third Affiliated Hospital of Shenzhen University, Shenzhen, China
[c] Department of Clinical Medicine, Shantou University Medical College, Shantou, China

ARTICLE INFO

Keywords:
Case report
Loeys-Dietz syndrome
Transforming growth factor-beta
Molecular dynamics

ABSTRACT

Introduction: Loeys-Dietz syndrome (LDS) is a rare autosomal dominant disorder with extensive connective tissue involvement. The diagnosis of this disease is mainly based on clinical features combined with the detection of pathogenic gene mutations, mainly mutations in the transforming growth factor-beta (TGF-β) signaling pathway.

Methods: The molecular pathogenesis of a LDS syndrome proband and his family members was analyzed using whole exome sequencing and validated using Sanger sequencing. Molecular dynamics simulations and in vitro cell experiments further analyzed the structural changes and functional abnormalities of the variation.

Results: This study describes the case of a 6-month-old infant diagnosed with LDS with typical craniofacial abnormalities, developmental delay, and a dilated aortic sinus (19 mm; Z-score 3.5). Genetic analysis showed the patient carried a novel de novo TGF-β receptor 2 (TGFBR2) mutation (NM_003242: c.1005_1007delGTA (p.Glu335_Tyr336delinsAsp)). Molecular dynamics simulation showed that the TGFBR2 c.1005_1007delGTA mutation changed the protein conformation, making the protein conformation more stable. The p.Glu335_Tyr336delinsAsp mutation significantly reduced TGF-β-induced gene transcription and phosphorylation of SMAD Family Member 2 (SMAD2) *in vitro*.

Conclusions: Our comprehensive genetic analysis suggested that the p.Glu335_Tyr336delinsAsp variant of TGFBR2 caused aberrant TGF-β signaling and contributed to LDS in the patient.

1. Introduction

Loey-Dietz syndrome (OMIM#609192, LDS) is an autosomal dominant disorder of the connective tissue that is typically clinically characterized by aortic aneurysm or tortuosity, hypertelorism, and uvula fissure. LDS was first systematically described by Loeys et al. [1,2]. The cardiovascular and skeletal lesions of LDS are very similar to those of Marfan syndrome (MFS), but the growth rate of aneurysms and the risk of aortic rupture in patients with LDS are much higher than those in patients with MFS [3]. It should be noted that in LDS, aneurysms and arterial tortuosity can be founded throughout the entire arterial tree. Therefore, imaging beyond the aorta

* Corresponding author. Shenzhen Eye Hospital, Jinan University, Shenzhen Eye Institute, Shenzhen, Guangdong, China.
** Corresponding author. Shenzhen Eye Hospital, Jinan University, Shenzhen Eye Institute, Shenzhen, Guangdong, China.
E-mail addresses: xhualiu@sohu.com (X. Liu), wangjiantao65@126.com (J. Wang).
[1] The authors contributed equally to this paper.

https://doi.org/10.1016/j.heliyon.2025.e42116
Received 24 August 2024; Received in revised form 13 January 2025; Accepted 17 January 2025
Available online 18 January 2025

is of vital importance in LDS patients [4–6]. The average age at death in patients with LDS is significantly lower than that in patients with Marfan syndrome. Thus, it is important to determine the optimal timing for surgery in clinical practice [7].

Abnormal conduction of the transforming growth factor-beta (TGF-β) signaling pathway has been identified as the main pathogenic cause of LDS syndrome; the main involved genes are TGF-β receptor (TGFBR)-1, TGFBR2, TGFB2, TGFB3, and SMAD3 [4,8]. Therefore, the revised LDS diagnostic taxonomy classifies patients into five types based on the mutated gene: TGFBR1 (LDS 1), TGFBR2 (LDS 2), SMAD3 (LDS 3), TGFB2 (LDS 4), SMAD2 and TGFB3 (LDS 5) [9,10]. Approximately one-quarter of patients have a family history of mutation, while three-quarters have de novo mutations [11]. TGF-β signaling plays a crucial role in multiple biological processes such as skeletal development, angiogenesis, and hematopoietic homeostasis, and is essential for maintaining Extracellular matrix (ECM) homeostasis [12]. In addition to LDS syndrome, abnormal TGF-β signaling pathway is closely related to the occurrence of other heritable connective tissue disorders such as MFS, Ehlers-Danlos Syndrome, and Familial Thoracic Aortic Aneurysms and Dissections [13]. Many researchers have constructed point mutation, deletion, and insertion mouse models of TGFBR1, TGFBR2, SMAD3, and TGFB2, and confirmed that these gene mutations can lead to aortic abnormalities, cleft palate and calvaria defects, among other abnormal developmental phenotypes [14–18].

In the present study, we describe the case of an infant with LDS syndrome caused by a novel *de novo* heterozygous mutation in TGFBR2 (NM_003242: c.1005_1007delGTA (p.Glu335_Tyr336delinsAsp)). We aimed to determine the downstream signaling effects of these mutations in an effort to better understand their influence on LDS. We hope to expand our knowledge on the mutation spectrum of TGFBR2 in LDS and the pathogenesis of LDS syndrome, and to provide new clues for its clinical diagnosis.

2. Methods

2.1. Subjects

A six-month-old boy with a skeletal deformity and aortic dilatation visited our hospital for ocular screening for Marfan syndrome. Him and his family were used as the subjects of this work. This study was performed in accordance with the Declaration of Helsinki and was approved by the Ethics Committee of Shenzhen Eye Hospital (Approval Code: 2021110402-03). All individuals taking part in this research provided written informed consent.

2.2. Whole-exome sequencing (WES) and Sanger sequencing

All four participants underwent whole exome sequencing and the experimental process is briefly described as follows: approximately 5 mL of peripheral whole blood was collected from each participant using an EDTA anticoagulant tube, and genomic DNA was extracted using the MagPure Buffy Coat DNA Midi KF Kit (Qiagen, United States) according to the manufacturer's standard procedure. DNA library preparation and enrichment were performed according to previously described methods, and sequenced using the MGISEQ-2000 platform (BGI, Guangdong, China).

To refine the raw data, we undertook a process that eliminated adapter sequences and low-quality reads, thereby yielding high-quality clean data. We then employed the BWA alignment software to map this clean data against the human reference genome [19,20]. After alignment, we utilized the Picard tool (http://broadinstitute.github.io/picard/) to remove any duplicate reads. Further analysis was conducted using the Genome Analysis Toolkit (GATK), which included local re-alignment, base quality recalibration, and the detection of single nucleotide variants (SNVs), insertions/deletions (InDels), and genotypes. For the detection of copy number variations at the exon level, we used the ExomeDepth software. The annotation and prediction of the impact of identified mutations were carried out using SnpEff software, where we ascertained whether SNVs/InDels resulted in alterations to protein coding and amino acids. Additionally, we checked for the presence of these mutations in public databases such as the UCSC Genome Browser, dbSNP, ClinVar, 1000Genome, ExAC, TOPMED, and gnomAD. In our analysis, we excluded SNVs that had a Minor Allele Frequency (MAF) greater than 1 % as reported in the Thousand Genomes Project. In addition, nonsynonymous single nucleotide variants (SNVs) underwent further analysis by being submitted to PolyPhen-2 (Polymorphism Phenotyping v2) and PROVEAN (Protein Variation Effect Analyzer) for functional prediction. According to the guidelines provided by the American College of Medical Genetics and Genomics (ACMG) classification, the clinical significance of identified variants has been interpreted. Screening candidate variants based on clinical information of the subjects and verifying the authenticity of the identified candidate variants through Sanger sequencing, as well as conducting family co isolation verification. The primer sequences for TGFBR2 verification were 5′-CAACCACAACACAGAGCTGC-3′ and 5′- TCACACAGGCAGCAGGTTAG-3′.

2.3. Molecular dynamics (MD) simulations

The structural file of TGFBR2 (PDB code: 1OKI) was downloaded from the Protein Data Bank and the E335_Y336delinsD variant was constructed using PyMOL, a molecular graphics system (http://www.pymol.org/). All simulations were performed using GROMACS (version. 2018.4) under the CHARMM27 force field and TIP3P water model. The steepest descent method was used to minimize the energy of the two systems and to eliminate excessive contact between atoms. Next, the system was equilibrated for 100 ps under NVT and NPT conditions at 300 K. Finally, the simulations were run at 2 fs time steps for 200 ns. During MD simulation, all hydrogen bonds were constrained using the LINCS algorithm. The simulated courses were processed and analyzed using Visual Molecular Dynamics (version 1.9.3.20). The backbone root mean square deviation (RMSD), backbone root mean square fluctuation (RMSF), and solvent-accessible surface area (SASA) were analyzed using GROMACS.

2.4. Cell culture and transfection

HCT116 cells were cultured in 5a medium supplemented with 10 % fetal bovine serum (Gibco, Carlsbad, CA, USA) and 1 % penicillin/streptomycin under humidified air containing 5 % CO2 at 37 °C. Human wild-type (pCDNA3.1-TGFBR2-WT-flag) and mutated (pCDNA3.1-TGFBR2-MUT-flag) plasmids were constructed by General Biology Technology Company for detection of ectopic expression of TGFBR2 protein, dual-luciferase reporter assay and TGFB1 stimulation assay. p3TP-Lux reporter plasmid containing TGF-β responsive elements were purchased from Addgene (www.addgene.org/). When HCT116 cells reached 70 % confluency, wild-type or mutant plasmids were transfected into cells simultaneously with plasmid p3TP-Lux using lipofectamine 3000 reagent (Thermo Scientific, Shanghai, China). After 24 h, all cells were treated with serum-free medium containing 5 ng/mL TGF-β1 (Proteintech) or PBS for an additional 24 h. Cells were then collected and luciferase expression was measured using the Dual-Luciferase Reporter Assay System (Promega, Madison, WI, USA) according to the manufacturer's instructions. The total protein concentration was used to control the luciferase activity and experiments were performed in triplicate.

2.5. Western blotting

Cells were harvested and lysed using an ice-cold lysis buffer containing protease and a phosphorylation inhibitor (Beyotime Biotechnology). Extracted proteins were quantified using the BCA Protein Assay kit (Thermo Fisher Scientific) according to manufacturer's instructions, separated by 12 % sodium dodecyl sulfate-polyacrylamide gel electrophoresis (SDS-PAGE), and transferred onto polyvinylidene fluoride (PVDF) membranes (Bio-Rad, Hercules, CA, USA). After blocking with 5 % skimmed milk in Tris-buffered saline with 0.1 % Tween-20 (TBST) at room temperature for 2 h, the membrane was incubated with one of the following antibodies overnight at 4 °C: anti-Flag (catalog number: #66008-4-Ig; Proteintech), phosphorylated-SMAD2 (p-SMAD2) (catalog number: #3108;

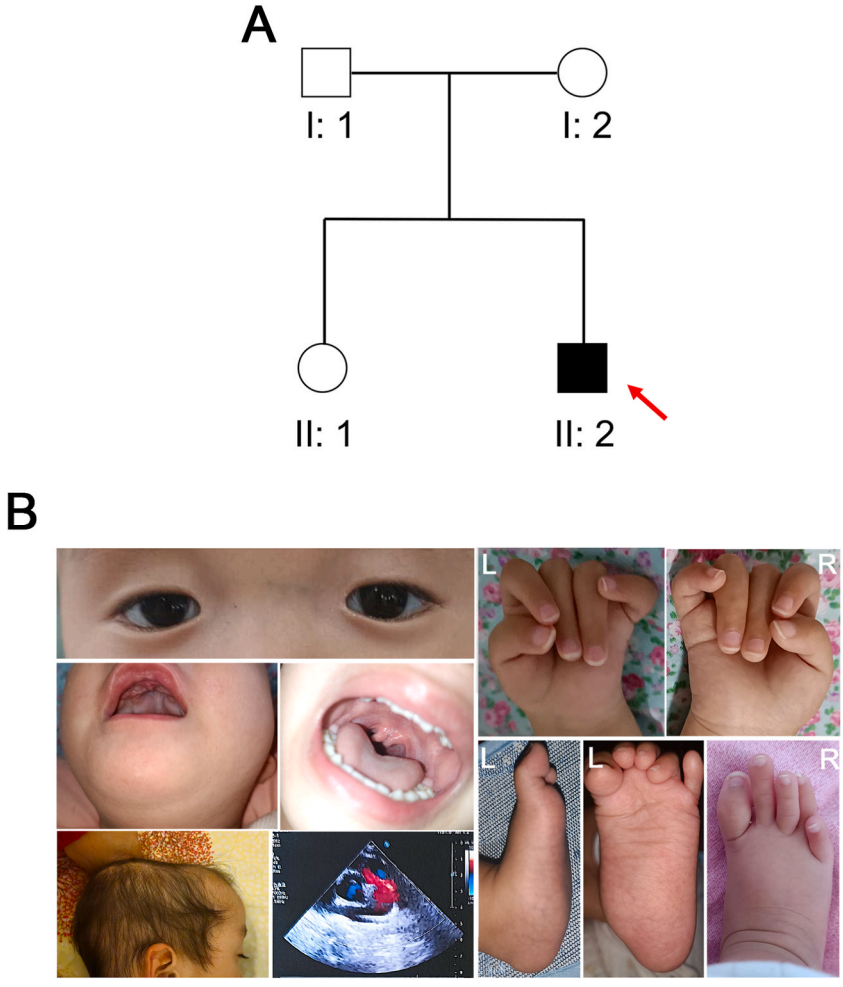

Fig. 1. Pedigree (A) and clinical characteristics (B) of the Chinese family with Loeys–Dietz syndrome. The image of cleft uvula was taken when the child was two years and two months old, and the image of scaphoid head deformity were taken when the child was one years and six months old. The proband is indicated by a red arrow.

Cell Signaling), SMAD2 (catalog number: ab40855; Abcam), anti-GAPDH (catalog number: ab9485; Abcam). Subsequently, the membranes were incubated with a horseradish peroxidase- - conjugated goat anti-rabbit IgG secondary antibody (catalog number: ab6721; Abcam) for 1 h at room temperature. Protein signals were visualized using an electrochemiluminescence reagent (Thermo Fisher Scientific). Protein band intensities were quantified using ImageJ software (version, 1.8.0_172; National Institutes of Health).

3. Results

3.1. Clinical features of the family

In this study, a six-month-old male infant was admitted to our hospital for eye examination because of suspected MFS. The infant's father and sister were had no health issues; the mother had suffered from lumbar and joint pain since childhood, and was diagnosed with lumbar disc herniation (Fig. 1A). Physical examination showed that the infant had a widened interorbital distance (4.1 cm), a high arch and uvula cleft, long deformed fingers and toes, and a severe vertical talus in his right foot (Fig. 1B). During a follow-up one year later, we found that the patient had a severe scaphoid head deformity (Fig. 1B). At about 1 years and 7 months old, the patient underwent vertical talus correction surgery and treatment surgery for craniosynostosis. A developmental examination of the children showed that his developmental level lagged behind that of normal children by approximately two months. Cardiac color Doppler ultrasound showed that the aortic sinus had widened (1.9 cm), with a Z-score of 3.5 (Fig. 1B). Other symptoms included inguinal hernia, bilateral frontotemporal space widening, bilateral ventricular subependymal cysts, and allergic constitution (image not shown). The patient is currently 2 years and 7 months old and received treatment with losartan at the age of 2. He undergoes a cardiac ultrasound every 3–6 months, and the last one performed in August 2024 showed an aortic sinus diameter of 2.6 cm.

3.2. Genetic investigations

A new deletion mutation in TGFBR2 (NM_003242: c.1005_1007delGTA) was identified in the infant through whole-exon sequencing, and the parents of the infant were absent of the variant. With this mutation, glutamic acid at position 335 and tyrosine at position 336 had become aspartic acid (p.Glu335_Tyr336delinsAsp) (Fig. 2A). These sites are evolutionarily conserved across multiple species (Fig. 2B). This mutation, located in the TGFBR2 kinase domain, shortened the TGFBR2 protein by one amino acid (Fig. 2C). According to the ACMG guidelines, this mutation is located in the hotspot mutation region and has not been reported in the ESP database, the 1000 People database, or in the normal control population of the EXAC database. Therefore, this mutation was defined as a likely pathogenic mutation in LDS. The protein structures of TGFBR2 and TGFBR2 with the Glu335_Tyr336delinsAsp mutation are shown in Fig. 2D.

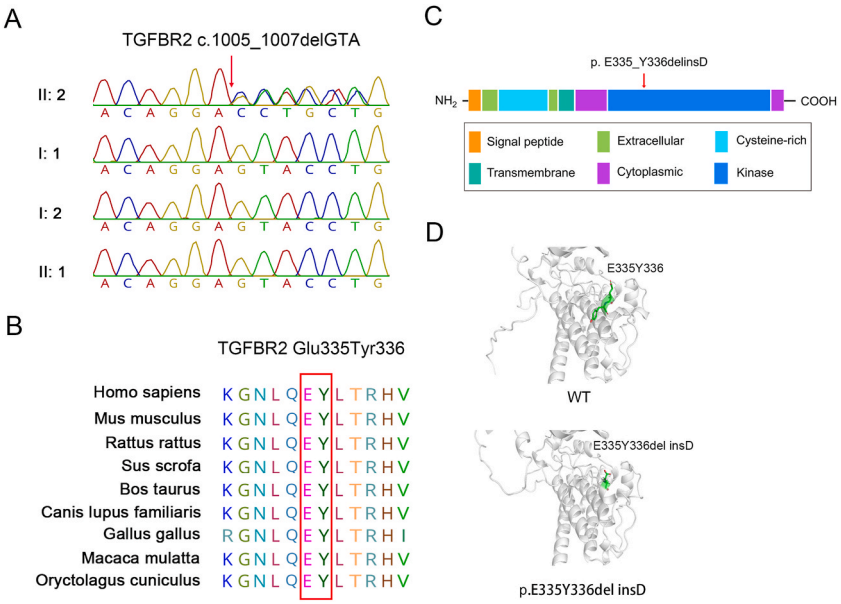

Fig. 2. Sequencing analysis and protein sequence conservation comparison of TGFBR2. (A) A missense mutation (TGFBR2 c.1005_1007delGTA) in the affected individuals (II: 2) is indicated by a red arrow (left). (B) Glutamine and tyrosine at the335th and 336th position in TGFBR2 (marked with a red wireframe) are highly conserved among different species. (C) The domain structure of TGFBR2 and Glu335_Tyr336delinsAsp mutation is located in the kinase domain. (D) Close up views of the TGFBR2 mutation site.

3.3. Molecular dynamics (MD) simulations

MD simulations were performed to monitor the effects of the Glu335_Tyr336delinsAsp mutation on the structural stability of TGFBR2. The TGFBR2 protein domain from 240 to 543 amino acid were used for Molecular dynamics analysis. The RMSD value, radius of gyration, and SASA of the mutant protein system were different from those of the wild type (WT) protein (Fig. 3A–C) indicating that the stability and tightness of the protein conformation changed after mutation. The regions with significant differences between the two proteins included F279-L299, A329-H339, and L429-E436 (Fig. 3D). The helix of the mutant protein was shorter than that of the WT protein (Fig. 3E). In addition, Glu335 formed two hydrogen bonds with adjacent Thr338 and Arg339, Tyr336 formed two hydrogen bonds with adjacent Arg339 and His340, and the carboxyl group on the main chain of Asn332 formed one hydrogen bond with Glu335 and Tyr336 in the WT system, whereas in the mutant protein, Asp335 only formed two hydrogen bonds with adjacent Arg339 (Fig. 3F). In contrast to the WT system, the carbonyl groups in the main chain and side chains of Asn332 in the mutant system formed hydrogen bonds with Asp335 (Fig. 3F). Further, the side chain of Asn332 may participate in substrate binding; therefore, the

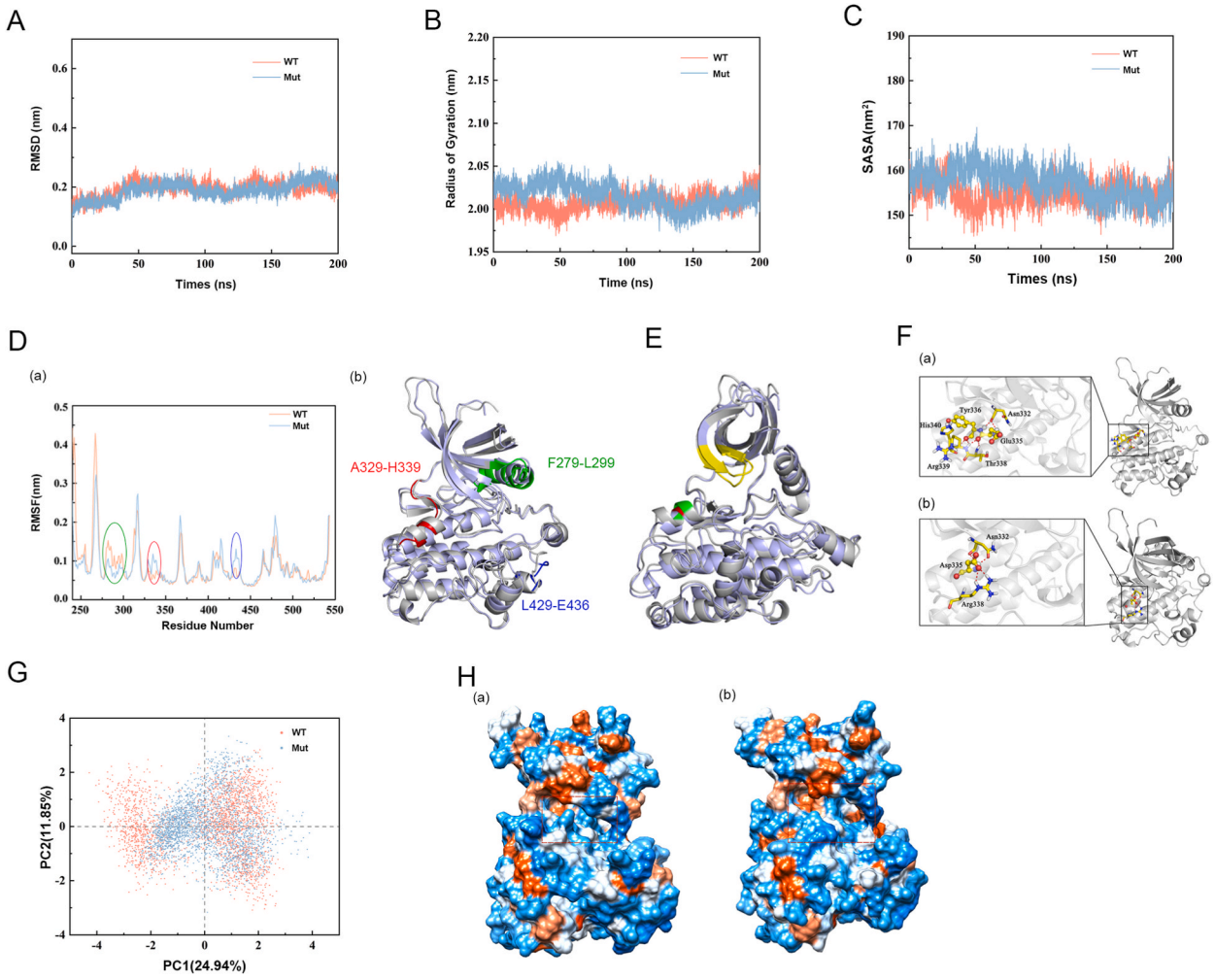

Fig. 3. (A–C) The time-course backbone RMSD, radius of gyration, and SASA values from the simulation structures for 100 ns. (D) The RMSF of amino acid residues in WT and mutant proteins (residue 0 to 300) (a) and the position of regions with significantly differences in the complex structure (b) (gray cartoon represents WT, and blue gray cartoon represents mutant; blue is the l190-e197 area, red is the a90-h100 area, and green is the f40-l60 area). (E) Secondary structure comparison of WT and mutant TGFBR2 proteins (gray cartoon represents WT, blue gray cartoon represents for mutant; green and red are used for WT and mutant mutation sites, respectively, and yellow for ATP binding sites). (F) The binding pattern of Glu335 and Tyr336 amino acids with surrounding amino acids in the WT protein (a); the binding mode of Asp335 amino acids with surrounding amino acids in the mutant protein (b). The bat model represents Glu335, Tyr336, and Asp335, respectively; the stick model represents the amino acids interacting with Glu335, Tyr336, and Asp335. The C atom is represented by yellow; the O atom is represented by red; the N atom is represented by blue; the H atom is represented by gray; and the red dotted line represents hydrogen bonding. (G) Principal component analysis of the WT and mutant proteins. (H) WT (a) and mutant (b) proteins distributed on the hydrophilic and hydrophobic surfaces (blue indicates the hydrophilic region, orange indicates the hydrophobic region), and the positions of active site cavities are framed by red dotted lines.

conformational change of amino acids near the binding site may directly affect the biological function of the enzyme [21]. Through principal component analysis on the atoms on the protein skeleton, it was found that the conformational changes of the entire WT protein system were significant, while the mutated protein system conformation was relatively stable (Fig. 3G). The hydrophilic and hydrophobic surface distributions of WT and mutant proteins were studied. The binding site cavity of the WT protein was smaller, but the protein cavity became larger after mutation, which may have led to an increase in the degree of freedom of movement of the substrate at the protein active site, making its binding unstable (Fig. 3H). In general, through MD simulation, we found that the Glu335_Tyr336delinsAsp mutation changed the hydrogen bond network and structural conformation near the active site of the TGFBR2 protein, and that the protein cavity became larger after mutation.

3.4. Functional assays of the TGFBR2 (NM_003242) c.1005_1007delGTA mutation

In order to detect the effects of TGFBR2 (NM_003242) c.1005_1007delGTA mutation on the TGF-β signaling pathway, we analyzed the downstream transcriptional activation characteristics through a luciferase reporter vector and phosphorylation detection of SMAD2 *in vitro*. First, the luciferase reporter construct containing a TGF-β responsive element that drives luciferase expression (p3TP-Lux) was co-transfected with WT or c.1005_1007delGTA TGFBR2 plasmid into HCT116 cells with endogenous TGFBR2 deficiency [22]. The fluorescence intensity of the WT and mutation groups with or without TGF-β1 stimulation was detected by fluorometer; the c.1005_1007delGTA variant significantly reduced the transcriptional activation of TGFBR2 regardless of TGF-β1 stimulation (Fig. 4B). Moreover, WT and mutated TGFBR2 expression levels had been detected by Western blot, and the results showed that there was no significant difference in the protein expression level in both groups (Fig. 4A). However, the phosphorylation level of SMAD2 protein in the mutant group was significantly lower than that of the WT group, regardless of TGF-β1 stimulation. This result indicates that the mutation destroys the function of TGFBR2, resulting in the interruption of the TGF-β signaling pathway (Fig. 4C).

4. Discussion

LDS is an autosomal dominant connective tissue disease characterized by abnormalities in the craniofacial region, skeleton, skin, and blood vessels, leading to aortic aneurysm and dissection. LDS was first described in 2005 [1,4]. Patients with LDS usually undergo echocardiography at regular intervals to monitor their heart status and prevent vascular accidents [9]. The clinical phenotype of LDS overlaps to some extent with MFS, including aortic root aneurysm, thoracic deformity, and scoliosis; however, there are also many differences between the two. For example, LDS is often accompanied by uvula cleft or cleft palate, widening eye distance, and aortic aneurysm with tortuosity [1,23]. Compared with MFS, LDS patients usually do not exhibit significant excessive growth of the long bones or lens dislocation, and LDS patients with aortic aneurysm or dissection have faster clinical progression and poorer prognosis with nonsurgical treatment [3]. Additionally, LDS patients exhibit a widespread condition of aortic aneurysms and tortuosity, with a notably higher incidence of vertebral artery tortuosity compared to patients with Marfan syndrome [4–6]. The molecular diagnosis of LDS is established by identifying pathogenic variants in TGFBR1, TGFBR2, SMAD2, SMAD3, TGFB2, or TGFB3 genes, all of which are a

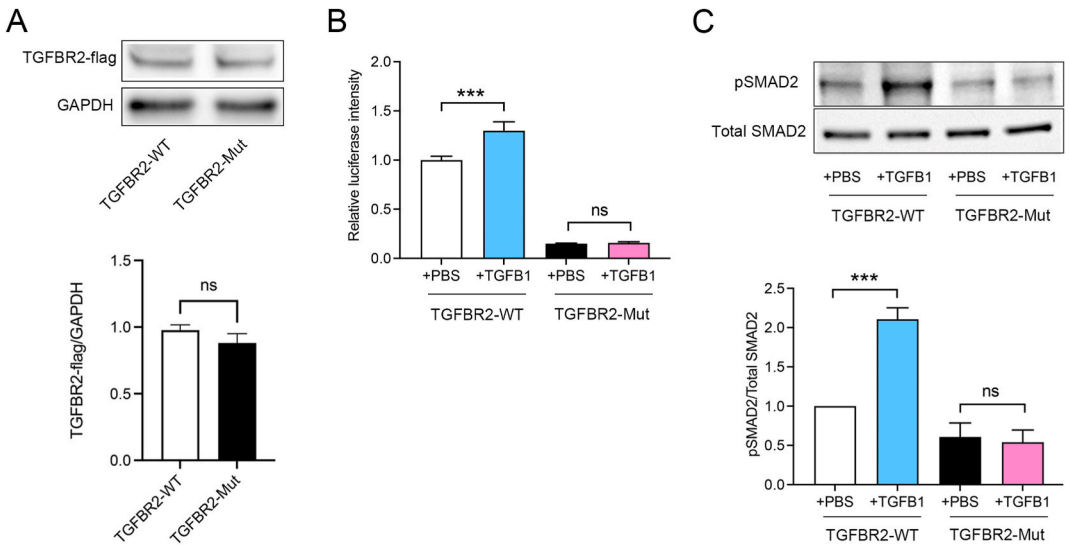

Fig. 4. TGFBR2 c.1005_1007delGTA mutation decreased canonical TGF-β signaling *in vitro*. (A) Representative western blotting images and the quantification of the Western blot density demonstrated that there was no significant difference in the protein expression levels of TGFBR2 between the TGFBR2-mutant group and the wild-type group. (B) Overexpression of TGFBR2 c.1005_1007delGTA in TGFBR2-deficient HCT116 cells leads to decreased TGF-β-associated gene transcription as observed via Luciferase reporter assay. (C) Representative western blotting images and the quantification of the Western blot density demonstrated decreased phosphorylated SMAD2 following TGF-β1 treatment compared with the wild type. N = 3, ***$p < 0.001$.

part of the TGF-β signaling pathway that is widely involved in cell differentiation, and the development of the skeletal and cardiovascular systems [9,24]. Nearly 80 % of all LDS cases are caused by mutations in TGFBR1 or TGFBR2 [4,25].

In this study, we identified a six-month-old LDS type 2 infant with classic clinical features of a highly vaulted palate, wide ocular distance, and uvula fissure, as well as widening of the aortic sinus, contracted finger joints, adduction deformity of the thumbs, and an allergic constitution. Whole-exome sequencing identified a de novo mutation in TGFBR2 (NM_003242: c.1005_1007delGTA (p.Glu335_Tyr336delinsAsp)). Previously, higher craniofacial severity index (CFI) scores were found in patients with LDS harboring TGFBR1 or TGFBR2 disease-causing variants [24]. The CFI score is correlated with the severity of aortic aneurysm pathology and inversely correlated with age at the first event [24,26]. To the best of our knowledge, this is the youngest case of LDS with aortic abnormalities reported in China; however, a 3-month-old American infant with aortic dissection was diagnosed with LDS [27]. One report showed that LDS 2 is the more aggressive subtype and recommend root surgery threshold of 4.0 cm [28]. Regalado and colleagues compared the risk differences for the first aortic event (either elective aortic aneurysm surgery or acute aortic dissection) across seven genes associated with heritable thoracic aortic disease: ACTA2, MYLK, PRKG1, TGFBR1, TGFBR2, SMAD3, and TGFB2, and they found that the cumulative incidence of type A aortic dissection in patients with TGFBR2 variants was lower than that in patients who underwent selective aneurysm surgery. Specific TGFBR2 variants are associated with a significantly increased risk of aortic events during childhood [29]. More than 91 % of TGFBR2 missense variants have been reported to be located in the kinase domain of both HGMD and ClinVar; the variation identified in this study is consistent [30]. The E335Y336 residue is highly conserved across multiple species, indicating that it may play an important role in protein function. In 2005, Loeys et al. [1] reported that three patients in one family with a TGFBR2 Y336N mutation had common symptoms of LDS syndrome, such as eye distance widening, uvula cleft, exotropia, pectus excavatum, clubfoot varus, visible skin transparent vessels, and aortic root aneurysm. One crucial mechanism of LDS may be changes in receptor function due to altered TGFBR2 protein conformation and inactivated kinase conformation, leading to downstream signaling pathway disorders [30].

By analyzing the changes in convergence parameters in the simulation process, MD experiments revealed that the conformation of the mutant protein system was more stable than that of the WT protein. This may make it more difficult for the mutant protein system to break the stable state to bind ATP. Further, the mutation changes the protein conformation and enlarges the protein cavity; these changes may interfere with the conformation of the transmembrane domain of TGFBR2 protein and damage TGF-β function of access.

The fluorescence enzyme assay using HCT116 cells showed that the mutation we discovered reduced TGF-β-related transcription and lead to a decrease in TGF-β-stimulated SMAD2 phosphorylation. SMAD2 is a target of the activated TGFBR1/2 complex. Phosphorylated SMAD2/3 forms stable trimeric complexes with SMAD4 and translocates to the nucleus to regulate target gene expression [31]. An abnormal balance in SMAD signaling is associated with the severity of disease phenotypes caused by TGFBR2 mutations [32]. Interestingly, analysis of tissue function in LDS patients found activation of the TGF-β signaling pathway, which is believed to be related to the dysregulation of inhibitory feedback mechanisms and compensatory activation of non-canonical pathways, but its more specific pathogenic mechanism remains to be further explored and verified [33,34]. This phenomenon could potentially occur in the pediatric patients included in this study, but it can only be confirmed by performing immunohistochemistry on a section of aortic tissue that is excised during prophylactic surgery.

5. Conclusion

In conclusion, we have reported a new case of LDS caused by a de novo mutation in TGFBR2. These findings expand the mutation spectrum of TGFBR2 linked to LDS, and provide new insights into understanding genotype phenotype correlations, contributing to accurate genetic counseling and treatment optimization. A major limitation of the study was that they were limited to in vitro assays, which may not fully recapitulate in vivo conditions. Further validation in the clinical samples of patients would be necessary to confirm the observed results.

CRediT authorship contribution statement

Xin Liu: Writing – review & editing, Writing – original draft, Visualization, Methodology, Investigation, Formal analysis, Data curation, Conceptualization. **Kaiqing Liu:** Writing – review & editing, Writing – original draft, Visualization, Methodology, Investigation, Formal analysis, Data curation, Conceptualization. **Lifu Hu:** Writing – review & editing, Validation, Resources, Data curation. **Zixiao Liu:** Writing – review & editing. **Xinhua Liu:** Writing – review & editing, Resources, Data curation, Conceptualization. **Jiantao Wang:** Writing – review & editing, Funding acquisition, Formal analysis, Conceptualization.

Data availability statement

Please contact author for data requests.

Ethics approval and consent to participate

This study adhered to the tenets of the Declaration of Helsinki and was approved by the Ethics Committee of Shenzhen Eye Hospital (Approval Code: 2021110402-03). Written informed consent forms were obtained from all investigated participants or his guardians who were under 18 years old.

Funding

We are grateful to the patients and their families for participating in the research. This work was funded by the National Nature Science Foundation of China (No. 82070961); Guangdong Provincial High-level Clinical Key Specialties (No. SZGSP014); the Shenzhen San Ming Project (No. SZSM202311012).

Declaration of competing interest

The authors declare that they have no known competing financial interests or personal relationships that could have appeared to influence the work reported in this paper.

Abbreviations

LDS	Loeys-Dietz syndrome
TGF-β	transforming growth factor-beta
MFS	Marfan syndrome
TGFBR	transforming growth factor-beta receptor
MD	molecular dynamics
WES	whole-exome sequencing

References

[1] B.L. Loeys, J. Chen, E.R. Neptune, D.P. Judge, M. Podowski, T. Holm, et al., A syndrome of altered cardiovascular, craniofacial, neurocognitive and skeletal development caused by mutations in TGFBR1 or TGFBR2, Nat. Genet. 37 (3) (2005) 275–281.
[2] L. Van Laer, H. Dietz, B. Loeys, Loeys-Dietz syndrome, Adv. Exp. Med. Biol. 802 (2014) 95–105.
[3] J.J. Maleszewski, D.V. Miller, J. Lu, H.C. Dietz, M.K. Halushka, Histopathologic findings in ascending aortas from individuals with Loeys-Dietz syndrome (LDS), Am. J. Surg. Pathol. 33 (2) (2009) 194–201.
[4] P. Gouda, R. Kay, M. Habib, A. Aziz, E. Aziza, R. Welsh, Clinical features and complications of Loeys-Dietz syndrome: a systematic review, Int. J. Cardiol. 362 (2022) 158–167.
[5] S.A. Morris, D.B. Orbach, T. Geva, M.N. Singh, K. Gauvreau, R.V. Lacro, Increased vertebral artery tortuosity index is associated with adverse outcomes in children and young adults with connective tissue disorders, Circulation 124 (4) (2011) 388–396.
[6] A.K. Kono, M. Higashi, H. Morisaki, T. Morisaki, Y. Tsutsumi, K. Akutsu, et al., High prevalence of vertebral artery tortuosity of Loeys-Dietz syndrome in comparison with Marfan syndrome, Jpn. J. Radiol. 28 (4) (2010) 273–277.
[7] L. Van Laer, D. Proost, B.L. Loeys, Educational paper. Connective tissue disorders with vascular involvement: from gene to therapy, Eur. J. Pediatr. 172 (8) (2013) 997–1005.
[8] H. Yang, Y. Ma, M. Luo, G. Zhu, Y. Zhang, B. Li, et al., Genetic profiling and cardiovascular phenotypic spectrum in a Chinese cohort of Loeys-Dietz syndrome patients, Orphanet J. Rare Dis. 15 (1) (2020) 6.
[9] G. MacCarrick, J.H. Black 3rd, S. Bowdin, I. El-Hamamsy, P.A. Frischmeyer-Guerrerio, A.L. Guerrerio, et al., Loeys-Dietz syndrome: a primer for diagnosis and management, Genet. Med. 16 (8) (2014) 576–587.
[10] D. Micha, D.C. Guo, Y. Hilhorst-Hofstee, F. van Kooten, D. Atmaja, E. Overwater, et al., SMAD2 mutations are associated with arterial aneurysms and dissections, Hum. Mutat. 36 (12) (2015) 1145–1149.
[11] B.L. Loeys, H.C. Dietz, Loeys-dietz syndrome, in: M.P. Adam, J. Feldman, G.M. Mirzaa, R.A. Pagon, S.E. Wallace, L.J.H. Bean, K.W. Gripp, A. Amemiya, W. A. Seattle (Eds.), University of Washington, Seattle Copyright © 1993-2024, University of Washington, Seattle. GeneReviews Is a Registered Trademark of the University of Washington, Seattle. All Rights Reserved, 1993. *GeneReviews(®)*.
[12] A.M. Bertoli-Avella, E. Gillis, H. Morisaki, J.M.A. Verhagen, B.M. de Graaf, G. van de Beek, et al., Mutations in a TGF-β ligand, TGFB3, cause syndromic aortic aneurysms and dissections, J. Am. Coll. Cardiol. 65 (13) (2015) 1324–1336.
[13] N. Takeda, H. Yagi, H. Hara, T. Fujiwara, D. Fujita, K. Nawata, et al., Pathophysiology and management of cardiovascular Manifestations in marfan and Loeys-Dietz syndromes, Int. Heart J. 57 (3) (2016) 271–277.
[14] Y. Ito, J.Y. Yeo, A. Chytil, J. Han, P. Bringas Jr., A. Nakajima, et al., Conditional inactivation of Tgfbr2 in cranial neural crest causes cleft palate and calvaria defects, Development 130 (21) (2003) 5269–5280.
[15] J. Iwata, J.G. Hacia, A. Suzuki, P.A. Sanchez-Lara, M. Urata, Y. Chai, Modulation of noncanonical TGF-β signaling prevents cleft palate in Tgfbr2 mutant mice, J. Clin. Invest. 122 (3) (2012) 873–885.
[16] I. van der Pluijm, N. van Vliet, J.H. von der Thusen, J.L. Robertus, Y. Ridwan, P.M. van Heijningen, et al., Defective connective tissue remodeling in Smad3 mice leads to accelerated aneurysmal growth through disturbed downstream TGF-β signaling, EBioMedicine 12 (2016) 280–294.
[17] M.E. Lindsay, D. Schepers, N.A. Bolar, J.J. Doyle, E. Gallo, J. Fert-Bober, et al., Loss-of-function mutations in TGFB2 cause a syndromic presentation of thoracic aortic aneurysm, Nat. Genet. 44 (8) (2012) 922–927.
[18] M. Dudas, J. Kim, W.Y. Li, A. Nagy, J. Larsson, S. Karlsson, et al., Epithelial and ectomesenchymal role of the type I TGF-beta receptor ALK5 during facial morphogenesis and palatal fusion, Dev. Biol. 296 (2) (2006) 298–314.
[19] H. Li, R. Durbin, Fast and accurate short read alignment with Burrows-Wheeler transform, Bioinformatics 25 (14) (2009) 1754–1760.
[20] H. Li, R. Durbin, Fast and accurate long-read alignment with Burrows-Wheeler transform, Bioinformatics 26 (5) (2010) 589–595.
[21] S. Miwa, M. Yokota, Y. Ueyama, K. Maeda, Y. Ogoshi, N. Seki, et al., Discovery of selective transforming growth factor β type II receptor inhibitors as antifibrosis agents, ACS Med. Chem. Lett. 12 (5) (2021) 745–751.
[22] J. Lee, S. Ballikaya, K. Schönig, C.R. Ball, H. Glimm, J. Kopitz, et al., Transforming growth factor beta receptor 2 (TGFBR2) changes sialylation in the microsatellite unstable (MSI) Colorectal cancer cell line HCT116, PLoS One 8 (2) (2013) e57074.
[23] B.L. Loeys, U. Schwarze, T. Holm, B.L. Callewaert, G.H. Thomas, H. Pannu, et al., Aneurysm syndromes caused by mutations in the TGF-beta receptor, N. Engl. J. Med. 355 (8) (2006) 788–798.
[24] A.L. Huguenard, G.W. Johnson, R.R. Desai, J.W. Osbun, R.G. Dacey, A.C. Braverman, Relationship between phenotypic features in Loeys-Dietz syndrome and the presence of intracranial aneurysms, J. Neurosurg. 138 (5) (2023) 1385–1392.
[25] F. Baldo, L. Morra, A. Feresin, F. Faletra, Y. Al Naber, L. Memo, et al., Neonatal presentation of Loeys-Dietz syndrome: two case reports and review of the literature, Ital. J. Pediatr. 48 (1) (2022) 85.

[26] G. Teixidó-Tura, R. Franken, V. Galuppo, L. Gutiérrez García-Moreno, M. Borregan, B.J. Mulder, et al., Heterogeneity of aortic disease severity in patients with Loeys-Dietz syndrome, Heart 102 (8) (2016) 626–632.
[27] A. Malhotra, P.L. Westesson, Loeys-Dietz syndrome, Pediatr. Radiol. 39 (9) (2009) 1015.
[28] K. Krohg-Sørensen, P.S. Lingaas, R. Lundblad, E. Seem, B. Paus, O.R. Geiran, Cardiovascular surgery in Loeys-Dietz syndrome types 1-4, Eur. J. Cardio. Thorac. Surg. 52 (6) (2017) 1125–1131.
[29] E.S. Regalado, S.A. Morris, A.C. Braverman, E.M. Hostetler, J. De Backer, R. Li, et al., Comparative risks of initial aortic events associated with genetic thoracic aortic disease, J. Am. Coll. Cardiol. 80 (9) (2022) 857–869.
[30] M.A. Cousin, M.T. Zimmermann, A.J. Mathison, P.R. Blackburn, N.J. Boczek, G.R. Oliver, et al., Functional validation reveals the novel missense V419L variant in TGFBR2 associated with Loeys-Dietz syndrome (LDS) impairs canonical TGF-β signaling, Cold Spring Harb Mol Case Stud 3 (4) (2017).
[31] C.J. David, J. Massagué, Contextual determinants of TGFβ action in development, immunity and cancer, Nat. Rev. Mol. Cell Biol. 19 (7) (2018) 419–435.
[32] D. Horbelt, G. Guo, P.N. Robinson, P. Knaus, Quantitative analysis of TGFBR2 mutations in Marfan-syndrome-related disorders suggests a correlation between phenotypic severity and Smad signaling activity, J. Cell Sci. 123 (Pt 24) (2010) 4340–4350.
[33] H. Hara, N. Takeda, T. Fujiwara, H. Yagi, S. Maemura, T. Kanaya, et al., Activation of TGF-β signaling in an aortic aneurysm in a patient with Loeys-Dietz syndrome caused by a novel loss-of-function variant of TGFBR1, Hum Genome Var 6 (2019) 6.
[34] P. Fortugno, R. Monetta, V. Cinquina, C. Rigon, F. Boaretto, C. De Luca, et al., Truncating variants in the penultimate exon of TGFBR1 escaping nonsense-mediated mRNA decay cause Loeys-Dietz syndrome, Eur. J. Hum. Genet. 31 (5) (2023) 596–601.